PHYSICAL REVIEW B VOLUME 52, NUMBER 11 15 SEPTEMBER 1995-I

Mechanism of melting in submonolayer films of nitrogen molecules adsorbed on the basal planes of graphite

F.Y. Hansen
Department of Physical Chemistry, Technical University of Denmark, FKI 206 DTU, DK-2800, Lyngby, Denmark

L.W. Bruch
Department of Physics, University of Wisconsin—Madison, Madison, Wisconsin 53706

H. Taub
Department of Physics and Astronomy, University of Missouri—Columbia, Columbia, Missouri 65221
(Received 15 March 1995; revised manuscript received 30 May 1995)

The melting mechanism in submonolayer films of N_2 molecules adsorbed on the basal planes of graphite is studied using molecular-dynamics simulations. The melting is strongly correlated with the formation of vacancies in the films. As the temperature increases, the edges of the submonolayer patch become atomically rough and vacancies are first created there. Then there is an onset temperature at which the vacancies penetrate into the patch. At an intermediate region of coverages $\sim$ 0.3–0.8 commensurate layers, there is sufficient free volume for the film to melt at that temperature. At higher coverages, $\sim$ 0.8–1.0 layers, a solid with defects is formed, and additional free volume must be created by higher energy mechanisms such as layer promotion for melting to occur; thus, the melting temperature rises with coverage. In contrast, for very small patches, the atomically rough zone penetrates the entire patch at a lower temperature where the film melts. The calculated melting temperatures are significantly lower than observed experimentally, indicating a severe fault in the potential model. A possible source of the discrepancy is identified.

I. INTRODUCTION

The melting point of commensurate submonolayer N_2 films on graphite has the interesting dependence on coverage shown in Fig. 1, where the results of two heat capacity determinations of the melting temperature as a function of coverage are plotted.[1,2] All coverages in this paper are given in terms of fractions ρ of a vacancy-free $\sqrt{3} \times \sqrt{3}$ commensurate monolayer. There appear to be three characteristic regions. At low coverages, up to say $\sim$ 0.3 layers, the melting temperature increases with coverage; then, in the range of coverages from $\sim$ 0.3 to 0.8 layers, it is virtually independent of coverage; in the region from 0.8 to 1.0 layer, there is a steep rise in the melting temperature. The magnitudes of the temperatures shown in Fig. 1 are also noteworthy. The 75 K of the 1.0-layer melting is distinctly higher than the triple point temperature (63 K) of three-dimensional (3D) N_2. The melting temperature of the half monolayer, $\simeq$ 48 K, is also higher than the 36-K estimate of the 2D triple point temperature obtained from scaling the 3D value by the ratio (0.4/0.7) of the triple point temperatures of the 2D (no corrugation) and 3D Lennard-Jones solids.

We report here a molecular-dynamics study of the melting in the submonolayer commensurate nitrogen films. The focus is on structural defects in the submonolayer solids and the mechanisms by which they are formed.

Similar melting point curves occur for submonolayer commensurate films of CO and Kr on graphite.[3] The nitrogen and carbon monoxide molecules form herringbone structures at low temperatures, which then undergo rotational disorder transitions to a hexagonal structure before melting. The coverage dependence of the melting temperature of the submonolayer hexagonal solid is similar for N_2, CO, and Kr.

Such a variation of the melting point is not restricted to films with a hexagonal symmetry. Recent heat capacity measurements by Alkhafaji and Migone[4] on submonolayer films of butane molecules on graphite also show a dependence of the melting point on coverage. The butane molecules form a herringbone structure at low temperatures, but there is no rotational disorder transition to a hexagonal structure. The film melts directly from the herringbone structure as verified by neutron diffraction.[5] The examples differ in the magnitude of the temperature drop from the complete monolayer melting point to the submonolayer melting point: it is $\sim$ 50% in the nitrogen films and $\sim$ 15% in the butane films.

The significant drop in the melting temperatures suggests that the mechanism of melting in submonolayer films is quite different from that in complete monolayer films. Since this phenomenon appears to be widespread for the commensurate layers (butane, in fact, is uniaxially incommensurate), it is of great interest to understand the mechanism by which order in the solid is destroyed. The N_2/graphite system is a convenient one in which to examine the issue because of the wide range of data that is available, the large ratio of the melting temperatures of the complete monolayer and half monolayer, and the

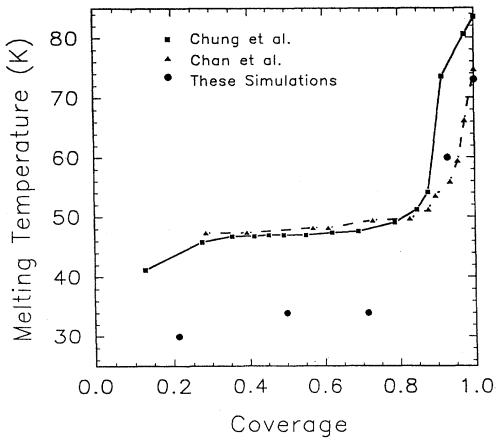

FIG. 1. The melting temperature of nitrogen films adsorbed on graphite as a function of coverage. The coverage is given as a fraction ρ of a vacancy-free $\sqrt{3} \times \sqrt{3}$ commensurate monolayer. The squares are the experimental results of Chung and Dash, Ref. 1, and the triangles the results of Chan *et al.*, Ref. 2. Differences near monolayer completion may reflect an uncertainty in the coverage determination due to some desorption of the film at high temperatures. The present simulation results are marked with a filled circle.

extensive modeling that has preceded our work.

Etters *et al.*[6] made Monte Carlo simulations of the N_2/graphite system and discussed the strong density dependence of the monolayer melting in terms of vacancy-induced melting. However, it was not feasible for them to examine the patch edges in the submonolayer and hence to identify the structural changes as the melting temperature is approached. We have combined Voronoi constructions with the strip geometry introduced for the submonolayer by Joshi and Tildesley[7] to demonstrate the existence and location of the vacancies. The relation of our work to some free-energy models of submonolayer phase diagrams for atoms and spherical molecules adsorbed on a corrugated surface is discussed briefly in Sec. V, where the vacancy description is contrasted to an emphasis on a modulated fluid phase.

We have already conducted studies of the melting mechanism in complete monolayer films of three rod-shaped molecules: nitrogen,[8] butane, and hexane.[9] The behaviors upon melting are quite different. Depending on the molecular aspect ratio, these examples display different ways in which sufficient free volume is created for the translational disorder to develop. Simulations of butane films showed that a tilt of the carbon backbone of the molecules away from the surface creates enough space to initiate the melting process. In films of hexane, with a larger aspect ratio of the molecules, this mechanism is too costly energetically; instead, the molecules coil up to form gauche configurations. By assuming a more globular shape, the molecules have a smaller footprint on the surface. For the nitrogen monolayer, the simulations showed that melting occurs only after the onset of appreciable promotion of molecules to a second layer.[6,8] However, the orientational disorder transition in the nitrogen film could be initiated by a small fraction of molecules tilting away from the surface to create enough space for the rotational disorder in the azimuthal angle of the N-N bond to develop. The difference between the rotational disorder transition temperature of $\sim$ 25–28 K and the melting temperature of $\sim$ 75 K for the nitrogen film reflects the energy difference between tilting a molecule in the first layer and promotion of a molecule to the second layer.

That the three-dimensional character of the motions is essential for understanding disorder transitions in molecular monolayers has also been demonstrated in simulations of incommensurate layers. Moller and Klein[10] noted the role of strongly tipped molecules in the melting of ethylene/graphite. Bhethanabotla and Steele[11] showed the coupling of temperature, density, and molecular orientation in the evolution of the oxygen/graphite system. In fact, the contrasting behavior in the N_2/graphite and O_2/graphite cases shows the limits of using a purely steric consideration such as the aspect ratio of the molecule to classify disorder transitions. The melting of the "low-coverage" δ-phase monolayer of O_2/graphite is accompanied by substantial tipping of molecules while for the (even lower density) commensurate N_2/graphite monolayer there is substantial layer promotion; yet the aspect ratios of O_2 and N_2 differ by less than 10%.

As already remarked, the drastic drop observed in the melting temperature of N_2/graphite from $\sim$ 75 K for the 1.0-layer film to $\sim$ 48 K at a coverage $\rho = 0.85$ indicates that the mechanism of melting is quite different in submomolayer films. The simulations reported here show that, indeed, the vacancy-forming mechanism is quite different from the one found in complete monolayer films. Vacancies are initially formed at the edges of the submonolayer islands, rather than by layer promotion. At low temperatures the adsorbed molecules coalesce and form patches or islands of molecules[6] with sharp and well-defined edges. Upon heating, the edges become atomically rough,[12] but the roughness initially penetrates only a limited distance into the patch. At a certain temperature, however, the vacancies permeate the entire patch. This appears to happen at the same temperature, for a wide range of coverages and patch sizes and leads to melting provided the mole fraction of vacancies is sufficient. Our simulations show a melting regime, which is independent of patch size and fractional coverage, in good agreement with experiments[1,2] in the coverage range of $\sim$ 0.3–0.8 layers. They also show the coverage dependence of the melting point at high coverages, which involves out-of-plane motions. The dense solid first develops defects and then melts after more free volume is created by processes such as the promotion of molecules to the second layer already seen in simulations of the 1.0-layer film. The melting temperature rises sharply at high coverages, since there is a smaller mole fraction of vacancies and the energy for layer promotion is much larger than the energy to create a vacancy in the submonolayer solid. There should also be a lowering of the melting temperature for very small patches, when the finite penetration depth of the edge roughness pervades the entire patch.

Joshi and Tildesley[7] made the pioneering molecular-

dynamics (MD) calculations on submonolayer films of nitrogen on graphite and demonstrated a dependence of the melting temperature on the corrugation in the molecule-substrate potential. Etters *et al.*[6] made a systematic Monte Carlo study of the melting point dependency on the coverage. They concluded that the melting transition was induced by vacancies and demonstrated that the melting temperature of the full monolayer was increased by 12 K if the molecules were constrained to a plane, but did not study the details of how vacancies were introduced in the submonolayer films.

Our calculated melting temperature of submonolayer N_2 films is 12–14 K below the observed melting temperature and indicates that there are severe faults in our potential model. We have analyzed this discrepancy in detail, using comparisons to the work of Joshi and Tildesley, and of Etters *et al.* We have concluded that the most likely source of the discrepancy is in the calculation of the McLachlan surface mediation of the intermolecular potential energy. If that term is set to zero, our results are in good agreement with experiments. There was also a hint of this problem in our complete monolayer calculations,[8] where the calculated azimuthal angle disorder temperature and melting temperature were a few Kelvins below the observed temperatures. (Distributing the McLachlan energy as an atom-atom interaction, as done in our simulations, adds a torque that competes with the ordering effect of the quadrupolar terms.) As yet, we have no resolution of this problem, although the calculation of the surface-mediated interaction has been critically reviewed.

The organization of the paper is as follows. Section II describes briefly the methods used in the calculations. Section III contains a summary of the interaction model. Section IV presents the results of the simulations. It is divided into four subsections. In the first we discuss the results of the simulations at an intermediate range of coverages, $\sim$ 0.3–0.8 layers, corresponding to the plateau region in the melting point curve and develop our picture of the mechanism of melting in submonolayer films. In the second, we discuss the results at high coverages, $\sim$ 0.8–1.0 layers, in the third, the results at small coverages, $\sim$ 0–0.3 layers, and in the fourth, the accuracy of the interaction model. Section V has some concluding remarks and summarizes our picture of the melting mechanism at coverages up to one layer.

II. CALCULATIONAL METHODS

The methods are the same as in our monolayer film calculation:[8] isothermal constrained molecular-dynamics calculations using Gears's fourth-order predictor corrector algorithm to integrate the equations of motion and with the N-N bond length fixed at its equilibrium value. A time step of 0.0025 ps was used; it gave a satisfactory energy conservation in a microcanonical (constant energy) simulation.

Simulations at coverages $\rho = 3/14$ (= 0.214), 7/14 (= 0.50), 10/14 (= 0.714), and 13/14 (= 0.929) have been performed with periodic boundary conditions in the x and y directions parallel to the basal planes of graphite. The graphite is treated as a static surface providing the external holding potential for the molecules. The initial configuration in all cases was the commensurate rectangular herringbone structure with lattice constants 7.38 Å and 4.26 Å, which is the low-temperature phase of the molecular solid. The simulation box is an almost square box with 8 7.38-Å lattice constants along the x axis (59.04 Å) and 14 4.26-Å lattice constants along the y axis (59.66 Å). This size was chosen to be on the scale of the coherence length $\sim$ 90–150 Å inferred for the graphite substrate in neutron scattering experiments on complete monolayer films of butane and hexane molecules.[9]

The reference frame used in the simulations has an origin at the center of a carbon hexagon. The x axis lies along the line from the origin to the midpoint of the hexagon edge. In the starting configuration, the nitrogen molecules form a rectangular patch with 8 7.38-Å lattice constants along $\hat{\mathbf{x}}$ and 3, 7, 10, and 13 4.26-Å lattice constants along $\hat{\mathbf{y}}$ corresponding to a coverage of 3/14, 7/14, 10/14, and 13/14 layers, and 48, 112, 160, and 208 molecules, respectively. The patch is positioned so that it forms a continuous band with its periodic images along $\hat{\mathbf{x}}$. The periodic images along $\hat{\mathbf{y}}$ are separated by a gap whose width depends on coverage. The configuration is illustrated in Fig. 2 for a coverage $\rho = 7/14$.

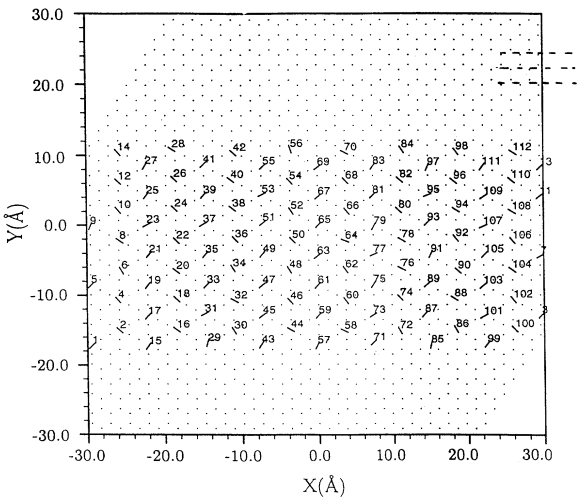

FIG. 2. The initial strip configuration in a $\rho = 0.5$ simulation. The small dots forming hexagons indicate the graphite carbon atom positions. The nitrogen molecules are shown as small lines, which represent the projection of the N-N bond on the xy plane parallel to the graphite surface. The origin of the xyz coordinate system is placed in the center of the central carbon hexagon in the simulation box, which extends from −29.52 Å to 29.52 Å along $\hat{\mathbf{x}}$ and from −29.826 Å to 29.826 Å along $\hat{\mathbf{y}}$. The patch is positioned in the middle of the simulation box and forms a continous band with periodic images along $\hat{\mathbf{x}}$. The periodic images along $\hat{\mathbf{y}}$ are separated by a gap with no molecules; the patch has free edges only along $\hat{\mathbf{y}}$. The binning geometry along $\hat{\mathbf{y}}$, which was used for generating density profiles and local structure factors, is indicated in the upper right corner.

This setup is similar to the strip geometry used by Joshi and Tildesley[7] for the $\rho = 0.5$ submonolayer film. A more realistic initial geometry is that used by Etters *et al.*,[6] in which the molecules are randomly positioned on the surface. Since Etters *et al.* found that the molecules coalesce to form one or a few large patches at temperatures below the melting point, the strip geometry appears to be more reasonable than first anticipated. Its advantage is that the patch has a well defined edge which makes it easier to analyze how the azimuthal angle disorder transition and the melting transition are initiated.

The systems were propagated in 100-ps time blocks, as explained in Ref. 8, typically for a total of 400 ps and near a transition for 800 ps.

III. INTERACTION MODEL

The interaction model is the same as in our complete monolayer simulations[8] and is summarized briefly here. We use the $X1$ model of Murthy *et al.*[13] fitted to 3D dense phase data. It consists of atom-atom interactions represented by a Lennard-Jones (12,6) potential and a distributed three-point-charge model for the electrostatic interactions between nitrogen molecules. The presence of the graphite introduces a three-body effect and modifies the 3D interaction. This substrate mediation of the intermolecular energy is represented by the McLachlan dispersion energy,[14] which typically constitutes 10–15 % of the intermolecular energy in a condensed monolayer phase. For molecules at the same distance above the surface, the energy is repulsive.

The molecule-substrate interaction is based on the Lennard-Jones (12,6) atom-atom potential for nitrogen-carbon interaction with Steele's parameters[15] supplemented with the anisotropy terms due to Carlos and Cole[16] to take into account the anisotropy of the graphite substrate. Furthermore, in order to fit neutron scattering data for the Brillouin zone-center frequency gap of the commensurate monolayer solid, we include an additional source of holding potential corrugation. Bonding in the graphite gives rise to aspherical atomic charge distributions, which are the source of electrostatic fields with rapid variations external to the graphite. X-ray data for the valence charge density of the bulk graphite were used to determine an effective quadrupole moment at each C atom in the graphite surface.[17]

IV. RESULTS

A. Intermediate coverages

Let us start with an analysis of the 0.5-layer simulation. At low temperatures, the nitrogen molecules form a herringbone structure as shown in the initial configuration in Fig. 2. The molecules are arranged in two sublattices with the N-N bonds parallel to the surface and the azimuthal angle of the N-N bonds at approximately $\pm 45°$ with respect to the 7.38 Å side (parallel to $\hat{\mathbf{x}}$) of the rectangular unit cell.

In the 1.0-layer simulations, there is a disorder transition of the azimuthal angle resulting in an ordered hexagonal lattice of the molecular centers. This transition also occurs in these submonolayer simulations. The temperature dependence of the orientational order parameters $o1 = \langle \sin(2\phi_1) \rangle$ and $o2 = \langle \sin(2\phi_2) \rangle$ for sublattices 1 and 2 is shown in Fig. 3. The angular brackets denote an ensemble average; ϕ_1 and ϕ_2 are the azimuthal angles on the two sublattices. The order parameters vary from $o1 = -o2 \simeq 1$ at low temperatures to zero at high temperatures where there is nearly free azimuthal rotation. In the range 15–20 K, both order parameters drop drastically and the curves have an inflection point around 18 K, which we identify as the disorder transition temperature. Also shown in Fig. 3 is the intensity of the (1,2) Bragg reflection for the herringbone superlattice defined by

$$S(\kappa_{h,k}) = \left\langle \sum_i \exp[i\kappa_{h,k} \cdot \mathbf{r}_i(\tau)] \times \sum_j \exp[-i\kappa_{h,k} \cdot \mathbf{r}_j(\tau)] \right\rangle, \quad (1)$$

for reciprocal lattice vectors

$$\kappa_{h,k} = 2\pi[h\hat{\mathbf{x}}/7.38 + k\hat{\mathbf{y}}/4.26] \text{ Å}^{-1}. \quad (2)$$

It, too, drops drastically in the temperature range 15–20 K with an inflection point at around 18 K. This transition temperature is somewhat lower than the 1.0-layer transition temperature of 22 K calculated for the same model. Thus, there also may be a change in the way the disorder transition is initiated in a submonolayer film. We shall return to that question later in this section.

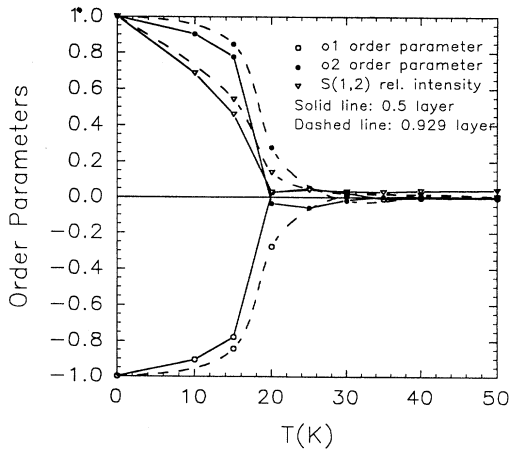

FIG. 3. Determination of the azimuthal angle disorder transition temperature for $\rho = 0.5$ and $\rho = 0.929$. The azimuthal angle order parameters $o1$ and $o2$ for sublattices 1 and 2 and the structure factor $S(1,2)$ of the herringbone lattice relative to its value at 0 K (4382 for $\rho = 0.5$ and 15 141 for $\rho = 0.929$) are plotted against temperature. There is an inflection point in both the order parameter and structure factor curves around 18 K, which is taken to be the transition temperature.

Figure 4 shows that the intensity of the $S(1,1)$ structure factor of the leading Bragg reflection drops drastically in the temperature range of 30–40 K, with an inflection point near 34 K. The intermolecular potential energy per molecule, also plotted in Fig. 4, shows a sharp rise in the same temperature region with an inflection point near 34 K; this is taken as the melting point of the 0.5-layer film. A comparison with the experimental results in Fig. 1 shows that the calculated melting point is significantly lower than the experimental value of $\sim$ 48 K. This is associated with a serious flaw in our potential model and will be discussed in more detail later in this section. Since we have been able to raise the $\rho = 0.5$ melting temperature from 34 K to about 45 K by adjusting the molecule-molecule interaction and still observe the same pattern of vacancy development, we believe that our interpretation of the mechanism of the melting is qualitatively correct.

To analyze the mechanism of melting, we first study a plot of the average distance z of the molecules from the surface. Figure 5 shows this distance as a function of the temperature. There is no marked rise in z at 34 K, the melting transition. This is in strong contrast to the behavior[8] in 1.0-layer films, where z rises sharply above 70 K. At 72 K, just prior to melting at 73 K, roughly 2% of the molecules of the 1.0-layer film are in the second layer (center-of-mass heights in the range 6–8 Å). The extra increment in z from 65 to 72 K closely matches to that anticipated from the increase in second-layer occupation. The melting mechanism in the complete monolayer film involves the promotion of molecules to a second layer to produce sufficient free volume for the film to melt.[6,8] Evidently, this does not occur at the lower temperature of the half-monolayer melting. Also shown in Fig. 5 is the average corrugation energy, i.e., the expectation value of

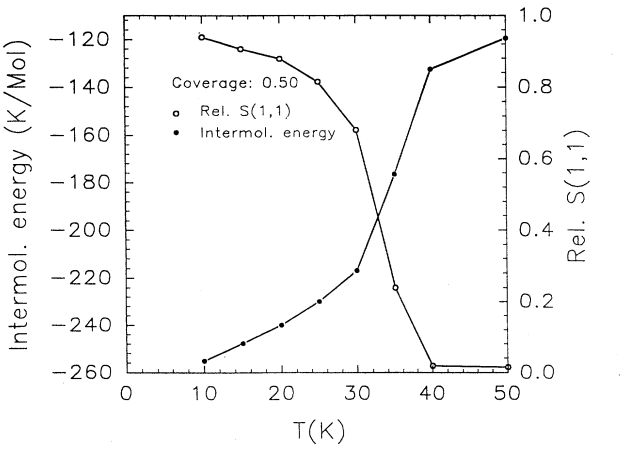

FIG. 4. Determination of the melting point for $\rho = 0.5$. The $S(1,1)$ structure factor, relative to its value at 0 K, 31 714, is plotted against temperature. The curve has an inflection point at around 34 K, which is taken to be the melting temperature. The intermolecular potential energy per molecule as a function of temperature, also shown, has a drastic increase in the same temperature region with an inflection point also near 34 K. The curves are smooth at 18 K, the azimuthal angle disorder transition temperature.

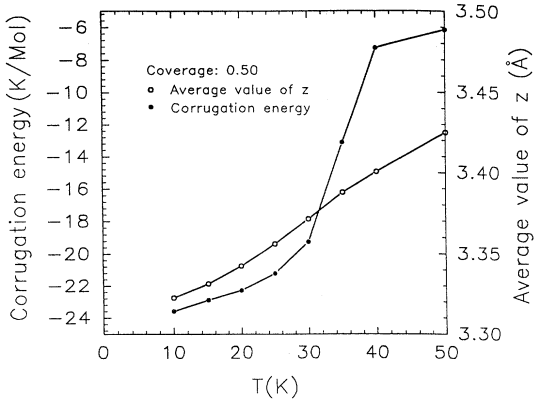

FIG. 5. The average distance z of the molecular center of mass from the surface and the average corrugation energy per molecule as a function of temperature for $\rho = 0.5$. The averages are defined in Ref. 8.

the laterally periodic terms in the nitrogen-graphite potential, defined as in Ref. 8. It has a steep increase at the melting transition, as for the complete monolayer. This rise and the very small inflection in z, barely visible in Fig. 5, both reflect the lateral motion, as discussed in Ref. 8.

The z distribution shows that layer promotion is not the mechanism for disordering the 0.5-layer film. We confirmed this in another calculation where the strength of the nitrogen-graphite interaction was drastically increased to constrain the molecules to the first layer. No increase in melting temperature was found. However, vacancies may be created in the submonolayer films by intraplanar motions. This is reflected in plots of the density profile along the $\hat{\mathbf{y}}$ direction of the patch. The y axis has been divided into bins, 2.13 Å wide, sampling the carbon atom hexagons as sketched in Fig. 2. Since there are eight herringbone lattice vectors along the $\hat{\mathbf{x}}$ axis, a perfect herringbone structure has eight molecules in each bin. At low temperatures, the density profile should have "sharp" edges, eight molecules per bin in the region of the patch, and zero molecules outside. This does occur: Figure 6 shows density profiles at a series of temperatures. Furthermore, the figure shows the onset of an atomic roughness of the edges when the patch is heated. The edges become less "sharp" and the roughness penetrates further inward into the patch as the temperature is increased until $\sim$ 34 K. Then the vacancies permeate the entire patch and the density decreases. That is, when a certain temperature is reached, the vacancies spread inward from the edges and the film melts provided that the concentration of vacancies is high enough.

To support this picture, we have constructed a series of Voronoi plots of instantaneous molecular configurations at different temperatures to show that there are no defects at the center of the patch below the transition temperature. In a Voronoi construction,[18] the lines from each molecule to its neighbors are drawn. In a perfect hexagonal crystalline structure, there will be six lines from each molecule (or vertex) marked by a dot in the graphs. The signature of defects is either a smaller or a

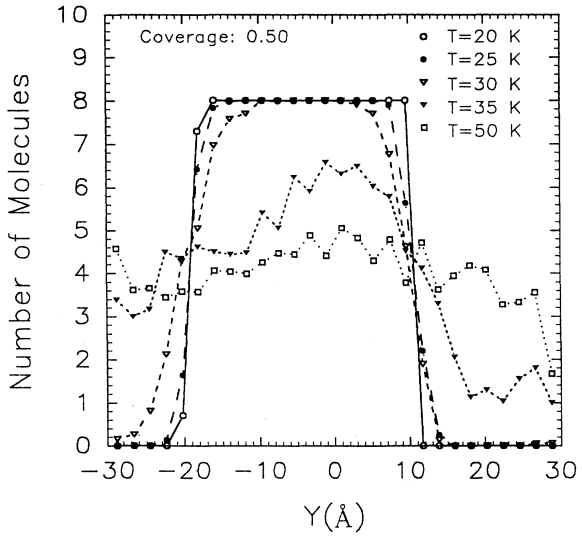

FIG. 6. The density profile of the ρ=0.5 layer film along $\hat{\mathbf{y}}$ at a series of temperatures.

larger number of tie lines from a molecule. Often they appear as pairs. The Voronoi plots in Fig. 7 show that no defects are generated in the interior of the patch at 30 K, below the estimated melting temperature of 34 K.

We examined the possibility that size effects may be important for these results by making a 0.5-layer simulation with a patch of 224 molecules, which is twice as wide along $\hat{\mathbf{y}}$ as the 112-molecule patch. The melting temperature is the same as for the 112-molecule patch, which seems to imply that size effects are unimportant in this case.

We have also analyzed the structure of the rough edges to find whether they are solidlike or fluidlike. This is done by calculating the $S(1,1)$ Bragg reflection intensity, averaged over four consecutive bins along $\hat{\mathbf{y}}$, as a function of y and normalized to the number of atoms in the four bins. The results, presented in Fig. 8, show that the structure of the rough edges is solidlike with defects, since the intensity is significantly higher than in the high-temperature fluid phase. Also note the drastic drop in the intensity going from 30 K to 35 K is consistent with a melting point at 34 K.

A similar analysis of the $S(1,2)$ Bragg reflection intensity has also been made to probe whether the azimuthal angle disorder also propagates inwards from the edges. Unfortunately, there was too much noise in the data for the bins in the edge region for us to decide whether the disorder is limited to an edge region until the transition temperature. An alternative analysis has therefore been made. In Fig. 9, we have plotted the azimuthal angle distributions for the 1.0- and 0.5-layer films, both at 15 K. The major peaks at 45° and 315° reflect the molecules in the two sublattices of the herringbone structure, and the smaller peaks at 225° and 135°, respectively, represent molecules that have rotated 180° in the azimuthal angle as explained in Ref. 8. The secondary peaks for $\rho = 0.5$ are much larger than for $\rho = 1.0$ at the same temperature and indicate a correspondingly higher degree of azimuthal angle disorder. We infer that the greater disorder is concentrated in the edge regions, since the polar angle distributions at 15 K (not shown here) are identical for $\rho = 0.5$ and $\rho = 1.0$. In turn, we conclude that at 15 K the interior of the patch is ordered, because the complete monolayer film simulations show that not until 22 K are enough molecules tilted away from the surface to produce free volume for a rotational disorder to develop. Hence the azimuthal angle disorder seems to propagate inwards from the edges at a transition temperature slightly lower than in a complete monolayer film. The argumentation is not as strong as for the inward motion of vacancies in the melting process, so the conclusion should be considered to be preliminary. The question will be analyzed in more detail in a forthcoming paper on the dynamical excitations in submonolayer films.

The results of the submonolayer simulations of a 0.714-layer film are very similar to those at 0.50 layer. Plots of the order parameters $o1$ and $o2$ and the $S(1,2)$ structure factor show a rotational disorder temperature at 18 K, as found at $\rho = 0.5$. This temperature remains constant at a value that is $\simeq$ 4 K below the transition temperature in the 1.0-layer solid. To our knowledge, this lowering of the orientational disorder temperature has not been observed experimentally. Analysis of the rotational disorder transition leads to the conclusion that the mechanism of disordering is the same as discussed above for $\rho = 0.5$. Furthermore, the melting point is the same as that in the 0.5-layer film: plots of the intensity of the $S(1,1)$ Bragg reflection relative to its value at 0 K and of the intermolecular potential energy both have an inflection point around 34–35 K as in Fig. 4 for the $\rho = 0.5$ case. The melting point is the same at coverages of 0.5 and 0.714 layers, in agreement with experiment. A plot of the local structure factor $S(1,1)$ as a function of y at a series of temperatures shows that the molecules in the rough zone near the edges can be characterized as a defect solid as in the $\rho = 0.5$ case. The Voronoi plots show that the defects move inwards from the edges as the temperature is increased and that they are not generated in the patch interior.

Our studies can be summarized in the following way. At low temperatures, the patches have sharp edges. When the patch is heated, the edges develop an atomic roughness. The edges become less sharp and the roughness penetrates further into the patch as the temperature increases. The penetration depth is finite until a temperature ($\sim$ 34 K for our model) where the penetration depth of the roughness becomes infinite, or said differently, vacancies then propagate from the edge regions of the patch into the patch interior. This seems to happen at the same temperature, over a range of coverage, and to reflect an energy-entropy balance. At low temperatures, the fuzziness is limited to a thin zone at the edges of the patch, since the energy cost for vacancies to propagate into the patch interior dominates over the entropy gain by mixing molecules and vacancies. Finally (at 34 K), the entropy of mixing balances the energy cost of propagating vacancies into the patch, and the film melts. This way of producing vacancies in the patch is very different from the layer promotion mechanism in the complete

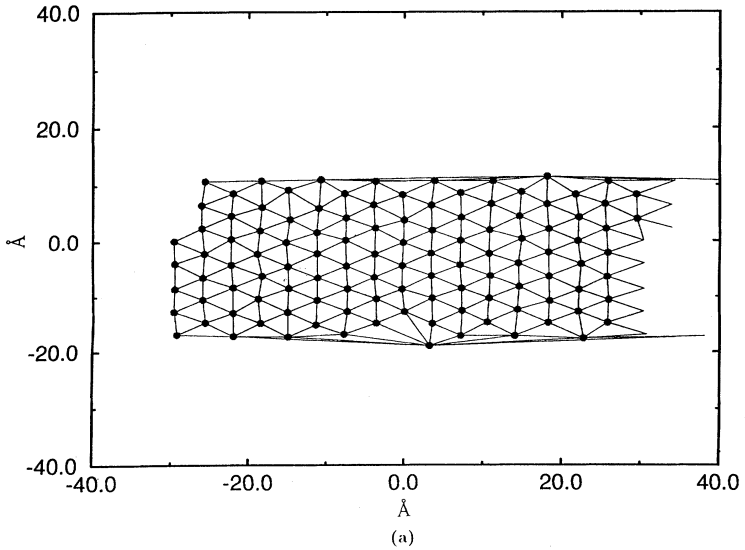

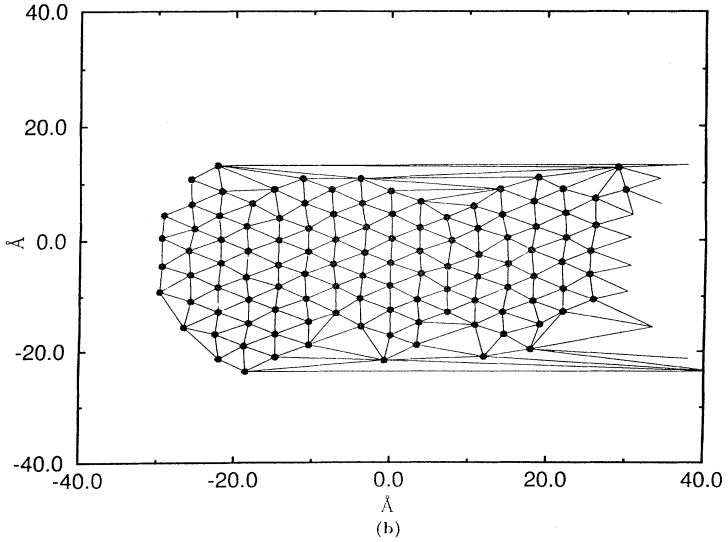

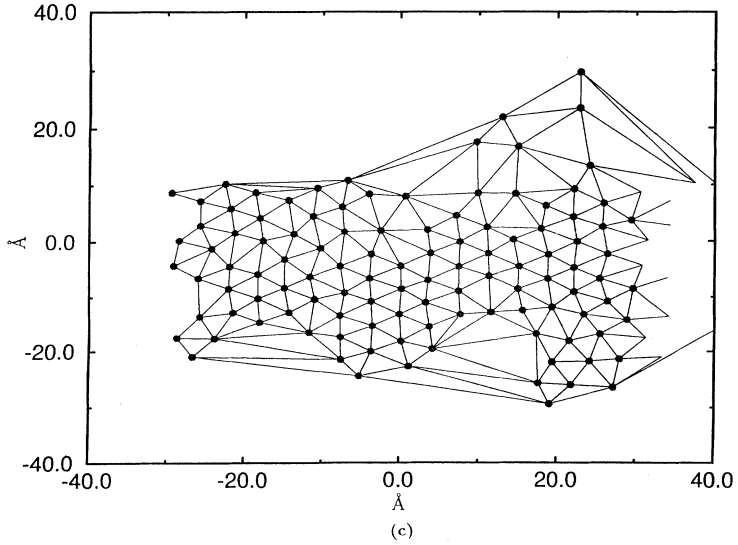

FIG. 7. Voronoi constructions of instantaneous molecular configurations for $\rho = 0.5$. The dots indicate the molecular center-of-mass positions. Defects are identified at positions where the numbers of tie lines are smaller or larger than six. (a) Well-ordered strip at $T = 20$ K; (b) vacancies present in edge regions at $T = 30$ K; (c) strip with vacancies in the interior at $T = 35$ K (a case which collapses to a fluid after further equilibration).

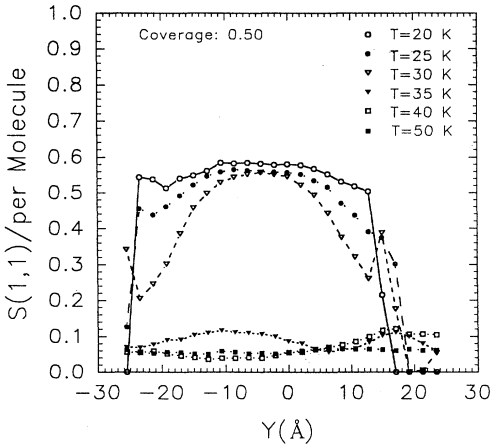

FIG. 8. The local $S(1,1)$ structure factor, normalized per atom, as a function of y and averaged over four consecutive bins along $\hat{\mathbf{y}}$ for $\rho = 0.5$.

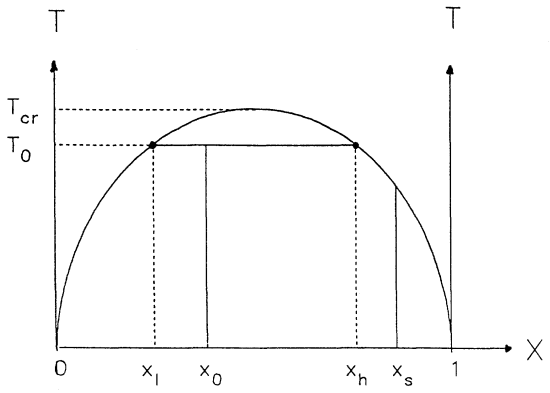

FIG. 10. A sketch of the miscibility gap for two partly miscible components. T is the temperature and x is the mole fraction of one of the components. T_{cr} is the critical temperature. See the discussion in Sec. IV A.

monolayer films.

An analogy to the thermodynamics of mixing helps to understand that the melting point of submonolayer films is independent of coverage. Consider two components (here, molecules and vacancies), which are partly miscible in some temperature region. A free-energy analysis would lead to a miscibility curve like the one sketched in Fig. 10, which shows the miscibility gap in a temperature-composition plot. At temperatures above the critical temperature, there is perfect miscibility of the two components independent of the overall composition. The system separates into two phases at temperatures below the critical temperature. The compositions of the two phases, for a given overall composition x_0 and temperature T_0, may be found by the tie-line construction shown in the figure and are given by x_l and x_h, respectively. Now let x represent the mole fraction of molecules on the surface, that is the coverage. The phase with the high mole fraction x_h then represents the molecular patch and the one with the small mole fraction x_l, the 2D gas phase. For the film to melt, a certain concentration of vacancies will be necessary, say $1 - x_s$. It is clear from the figure that, for any coverage less than x_s, the concentration of vacancies necessary for the film to melt is reached at the same temperature and thus there is a plateau in the melting point curve. Evidently, the $\rho = 0.5$ and 0.714 films have coverages less than x_s. In the next subsection, we show that the mixing analogy helps to understand the behavior at high coverages.

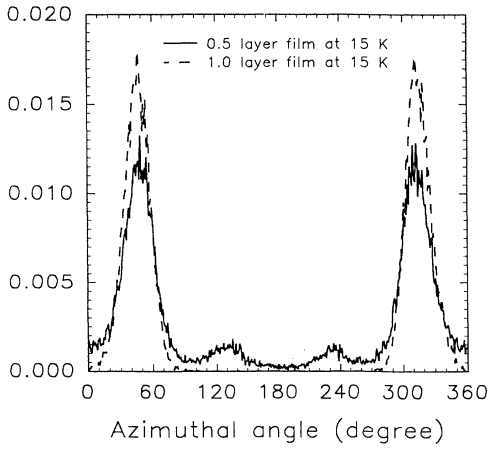

FIG. 9. The azimuthal angle distribution in nitrogen films at 15 K. The solid and dashed lines denote the distributions for ρ equal to 0.5 and 1.0, respectively. There is scarcely any strength in the $\rho = 1.0$ distribution for angles in the range 80°–280°.

B. High coverages

We use simulations of the 0.929-layer film to study the behavior of submonolayer films at high coverages. The plots of the order parameters $o1$ and $o2$ and the structure factor $S(1,2)$ in Fig. 3 are very similar to those for $\rho = 0.5$ and show that the rotational disorder transition temperature is still in the range 18–19 K. Thus, the azimuthal angle disorder transition temperature appears to be independent of the coverage even up to this high density. That this is not the case for the melting phenomenon is shown in Fig. 11: the graphs of both $S(1,1)$ and the intermolecular potential energy per molecule have inflection points at two temperatures, namely, near 35 K and near 60 K. This behavior, not seen at intermediate coverages, may be related to the occurrence of two features (at 49 K and 66 K) in specific heat data for $\rho = 0.975$.[2]

The plot of the average distance z of the molecules from the surface in Fig. 12 is nearly identical to that[8] for $\rho = 1$ up to about 60 K; but then at 65 K and 70 K, the z values are larger than for $\rho = 1$. The extra increment in z with increasing temperature, beyond the values extrapolated from lower temperatures, is primarily a consequence of an increase in second-layer population, from less than 0.1% of the total population at 60 K to about 0.3% at 65 K and 2% at 80 K. The plot of the corrugation energy shows both a jump near 35 K and a larger jump around

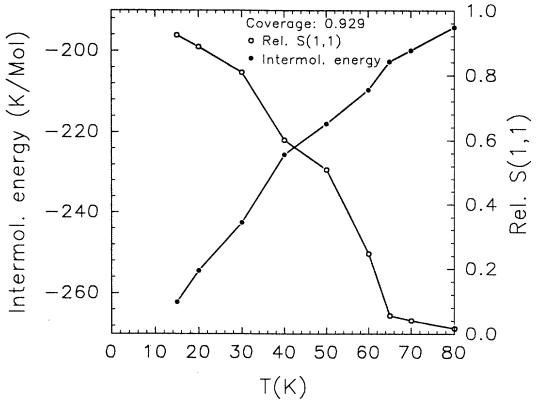

FIG. 11. Determination of the melting point for $\rho = 0.929$. The $S(1,1)$ structure factor, relative to its value at 0 K, 109 443, and the intermolecular potential energy per molecule are plotted as a function of temperature. Both curves show two inflection points, one near 35 K and one near 60 K. Both are smooth at 18 K, the azimuthal angle disorder transition temperature.

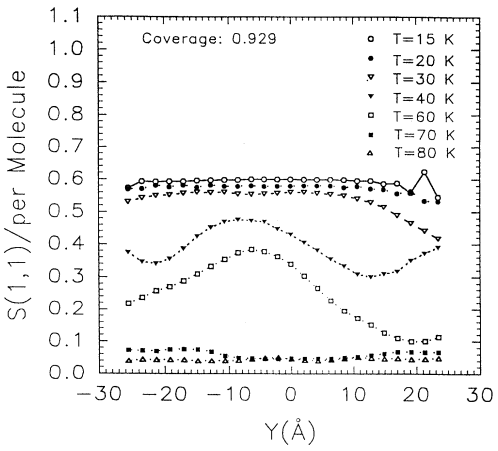

FIG. 13. The local $S(1,1)$ structure factor normalized per atom as a function of y and averaged over four consecutive bins along $\hat{\mathbf{y}}$ for $\rho = 0.929$.

60 K. This is consistent with the idea that near 35 K vacancies begin to propagate from the patch edges to the interior parts as at intermediate coverages. Density profiles, as in Fig. 6, show that the edges become more diffuse. However, the film has not melted, as the $S(1,1)$ structure factor is still quite large. Rather, there is a solid structure with defects. This is corroborated by the plot of the local structure factor $S(1,1)$ in Fig. 13. The drop in the magnitude of the structure factor in going from 30 to 40 K reflects the formation of the defect solid. The ensuing drop between 40 and 60 K is due to the Debye-Waller effect; a final large drop between 60 and 70 K leads to a magnitude characteristic of a fluid and is associated with the melting of the defect solid. The Voronoi plots in Fig. 14 show that defects penetrate to the patch interior at temperatures below 60 K. The feature in the specific heat data at 49 K, which coincides with the submonolayer melting point at intermediate coverages, may therefore reflect the onset of the mixing process of molecules and vacancies and the formation of a defect solid.

The melting mechanism in high-coverage submonolayer films can be summarized as follows. At the temperature corresponding to melting for intermediate coverages, vacancies permeate the interior parts of the patches, but the amount of free volume on the surface now is insufficient for the solid to melt. In terms of the thermodynamic mixing analogy, this corresponds to a coverage larger than x_s in Fig. 10. The one-phase mixture of molecules and vacancies may be characterized as a solid with defects. To provide the necessary free volume to melt the higher coverage layer, further processes must be activated. Our analysis of the average distance of the molecules from the surface shows that layer promotion is activated at a temperature close to that where the 0.929-layer film melts. We infer that at still higher coverages two mechanisms that contribute free volume for melting are the mixing of molecules and vacancies on the surface seen in the simulations for intermediate coverages and the layer promotion mechanism seen in the simulations of the 1.0-layer film. The activation energy of the former is smaller than that of the latter and they come into play at diferent temperatures. This results in a smooth transition in the melting temperature from the plateau region limited by the coverage x_s to a coverage of 1.0.

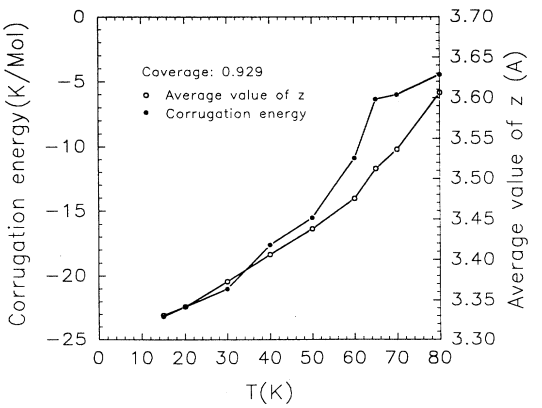

FIG. 12. The average distance z of the molecules from the surface and the average corrugation energy per molecule as a function of temperature for $\rho = 0.929$.

C. Low coverages

At low coverages, the melting point depends on the coverage. We find that the melting temperature is reduced for narrow strips, corresponding to a coverage of 0.214 layers. However, for small patches the shape of the patches is also relevant and we did not attempt to determine the exact range of "low-coverage" behavior, since that would require a study of the patch shapes formed at low coverages. Evaluation of the two order param-

eters $o1$ and $o2$ and the structure factor $S(1,2)$ shows that they are already vanishingly small (less than 0.1) at 5 K; such a low disorder transition temperature presumably depends on the shape of the patch. The $S(1,1)$ structure factor and the intermolecular potential energy per molecule, Fig. 15, both have an inflection point at around 28–30 K, taken to be the melting point. That this temperature is below the plateau value of around 34 K for our model is consistent with the experimental observation that the melting point of submonolayer films drops at small coverages. The density profiles in Fig. 16 provide an explanation. The lower melting point in the simulations arises because the roughness of the edge regions penetrates the entire patch at a temperature lower than the plateau temperature.

In summary, the coverage dependence of the melting point at small coverages is a size effect. The relationship between the onset of the drop in melting temperature and coverage is complicated and depends on the surface structure, coherence length of the substrate, and shape of the molecular patch. This work cannot throw light on this relationship, because it has been limited to a single perfect substrate structure and patch shape. It only demonstrates that the size effect in this particular setup is important at a coverage of 0.214 layers. At low coverages, there is a drastic reduction in the azimuthal angle disorder transition temperature; this too is a size effect.

D. Accuracy of the interaction model

In this section, we use a comparison of the calculated and observed temperatures to assess the accuracy of the interaction model. However, there are two reservations

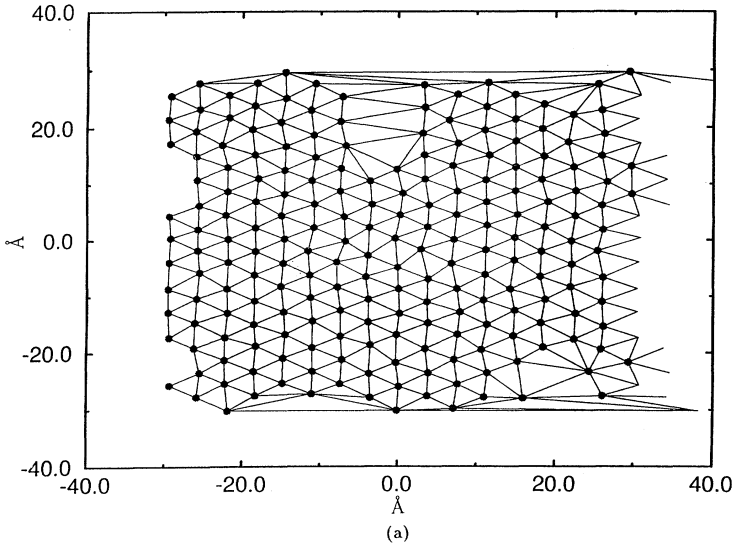

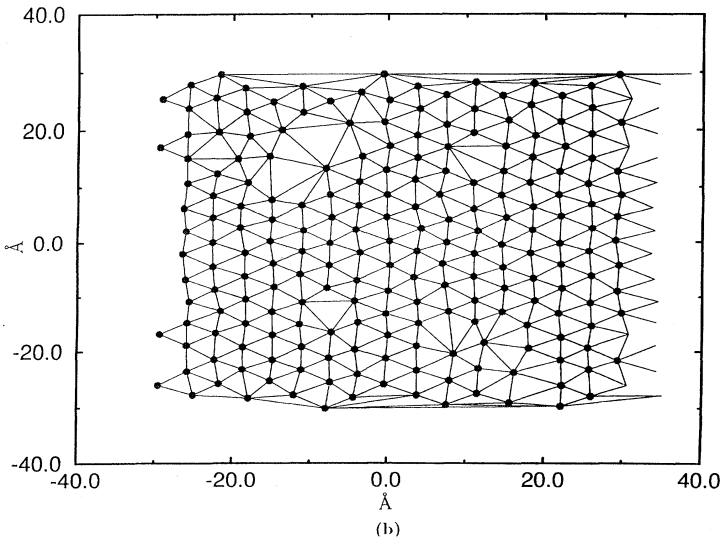

FIG. 14. Voronoi constructions of molecular configurations for $\rho = 0.929$. Identifications are in Fig. 7. (a) Defects at edge of strip, $T = 30$ K; (b) defects in the interior of the strip, $T = 40$ K.

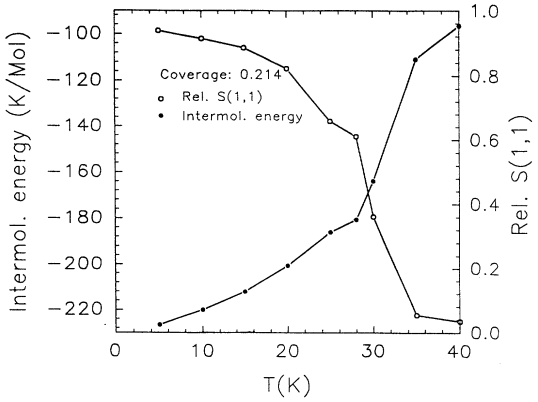

FIG. 15. Determination of the melting point in a $\rho = 0.214$ strip. The $S(1,1)$ structure factor, relative to its value at 0 K, 5826, is plotted against temperature. The curve has an inflection point near 30 K, which is taken to be the melting temperature. The intermolecular potential energy per molecule as a function of temperature, also shown, has a drastic increase in the same temperature region with an inflection point also near 30 K.

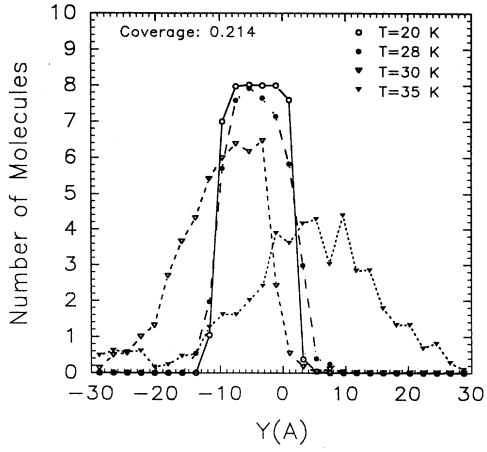

FIG. 16. The density profile at a series of temperatures for $\rho = 0.214$.

about the method of determining the calculated temperatures to be noted: (i) Taking the temperature of the inflection point in a plot to be the transition temperature may underestimate that temperature in view of the persistence of the calculated correlations to higher temperatures. (ii) Relying on the single-phase instability to signal the transition may overestimate the transition temperature because of metastability effects.

In our work on the melting transition in a complete monolayer film of nitrogen molecules on a graphite substrate,[8] we became aware of a possible fault in the interaction model. The calculated melting point at 73 K was in fair agreement with one set of experimental data and on the low side of another set. However, the calculated azimuthal angle disorder transition temperature at 22 K was lower than all the experimental values, which are in the range of 27–28 K. Since this transition depends more strongly on the intermolecular interactions than on the molecule-substrate potential, it appears that the intermolecular potential is too repulsive. Our submonolayer simulations support this conclusion.

We have summarized in Table I estimates of the melting temperature of the $\rho = 0.5$ layer for a variety of interaction models. The plateau melting point of 34 K in the present work is 13–15 K below the experimental value of 47–49 K. This supports the proposition that the inter-

TABLE I. Melting temperature for $\rho = 0.5$ layer of commensurate N_2/graphite for a variety of interaction models. The atom-atom interactions ϕ are either the $X1$ model of Murthy *et al.* (Ref. 13) or the KE model of Kuchta and Etters (Ref. 19), with N_2 quadrupole moment -1.173×10^{-26} erg cm^2 and -1.34×10^{-26} erg cm^2, respectively. The coefficients γ_A and γ_R are substrate anisotropy parameters introduced by Carlos and Cole (Ref. 16). The parameter Θ_s denotes the substrate electrostatic term of Hansen *et al.* (Ref. 17). The McLachlan interaction is as defined by Kuchta and Etters (Ref. 19). The melting temperature T_m is obtained as the point of inflection in the structure factor $S(1,1)$ or the intermolecular energy.

Case	ϕ	γ_A	γ_R	McL	Θ_s	T_m
JT1[a]	$X1$	0.	0.	no	no	39.5 ± 0.5
JT2	$X1$	0.4	-0.54	no	no	44.5 ± 0.5
JT3	$X1$	0.4	-0.9	no	no	≃ 47.5
JT4	$X1$	0.4	-1.05	no	no	≃ 48
N2F[b]	$X1$	0.4	-0.54	yes	yes	34
N2FA[c]	$X1'$	0.4	-0.54	yes	yes	43–45
KE1[d]	KE	0.4	-0.54	"no"	no	47–48
KE2[e]	KE	0.4	-0.54	yes	no	38–39

[a]JT1 to JT4 are results given by Joshi and Tildesley (Ref. 7).
[b]This work, with the interaction model constructed by Hansen *et al.* (Ref. 17).
[c]This work, adapted from N2F by changing the N-N Lennard–Jones interaction parameters to $\epsilon = 42.5$ K and $\sigma = 3.331$ Å.
[d]Kuchta and Etters,[6] with McLachlan energy effectively suppressed.
[e]Kuchta and Etters, private communication.

molecular potential is too repulsive, since we have shown that lateral motions of the molecules are essential for that transition. In order to localize the fault in our potential model, we made detailed comparisons with the work of both Joshi and Tildesley,[7] and Etters *et al.*,[6] since those authors found a better agreement with experiments than we did.

First, we checked our computations by repeating Joshi and Tildesley's simulation of a submonolayer film at a coverage of 0.5 layers using their setup of a patch of 140 molecules and their potential model (JT2 in the Table). It is the same as ours except for the McLachlan substrate-mediated energy[14] and the surface carbon atom quadrupole moment.[8,17] Neither of these terms was included in their model. We obtained exact agreement with their results at 35 K and also found the melting transition at 44 K as they did. Thus, there were no trivial errors in our computations. In order to bring the melting temperature to 47 K, for better agreement with experiments, Joshi and Tildesley adjusted the γ_R parameter in the expression for the anisotropic holding potential of Carlos and Cole[16] from a value of -0.54 to -1.04, thereby enhancing the corrugation in the holding potential. Our introduction of the surface quadrupole term also leads to an increased corrugation. Adding the McLachlan term and the carbon atom quadrupole moment to the JT2 model, we found a melting point at 34 K. Together these comparisons show that the cause of our low melting temperature is probably located in the McLachlan substrate-mediated-energy term. For the JT2 case, we found an intermolecular potential energy of -267 K/molecule compared to an energy of -176 K/molecule with our model, both at 35 K. That is, our potential is too repulsive because of the McLachlan term, which is repulsive. This causes the melting temperature to be too low. The McLachlan term is typically 15–17% of the intermolecular energy. However, its effect on the intermolecular energy at 35 K is much larger, because at this temperature the film is a solid for the JT2 potential model whereas it is a fluid in our model. In order to offset this repulsive term, we had to change the L-J parameters in the $X1$ model to the values given for case N2FA in the Table. However, we anticipate that this potential will give a poorer fit to the 3D results than the $X1$ model. The melting temperature of the submonolayer solid may be a very good test to discriminate between potential models.

We also performed a molecular-dynamics version of some of the Etters *et al.* Monte Carlo simulations,[6] using their intermolecular potential and four-point-charge model for the molecular quadrupole moment.[19] Our results agreed with theirs when we switched off the McLachlan term. While this term was included in their original computations, an error in the implementation caused it to give less than 1% of the interaction energy and to have no effect. When this was corrected, they found a melting point close to ours.[20]

All this indicates that there is a fault in the intermolecular potential and probably in the McLachlan term. The parametization of that term has been checked thoroughly but as yet we have not been able to propose a solution to the problem. The problem is even more puzzling in light of the fact that Bojan and Steele[21] found that surface virial coefficient data for N_2/graphite indicated the presence of an adsorption-induced repulsion on the scale of the McLachlan energy.

V. CONCLUSIONS

The behavior of submonolayer films of nitrogen molecules physisorbed on the basal planes of graphite has been studied with special emphasis on the mechanism of melting. We have found that as the temperature is increased from 0 K, a roughness of the edges of the patches develops. The penetration depth of the rough region increases with temperature, but is finite until a transition temperature is reached where it diverges. This is a result of a change in balance between the vacancy energy and entropy terms in the free energy. In analogy with the thermodynamics of mixing, there is a coverage-independent melting temperature provided that the concentration of vacancies is large enough. However, at high coverages additional free volume must be created by further processes such as the tilting of molecules and the layer promotion known from complete monolayer films.[6,8,10,11] These apparently have higher activation energies than that for intraplanar vacancy production in the submonolayer, and the melting temperature rises with increasing coverage.

Zhu, Pengra, and Dash[22] considered the possibility of edge melting, which would be the 2D analogue of surface melting. While we have clearly seen defects that nucleate at the edges of the submonolayer strips, we have no evidence that there is a fluid associated with them. The absence of evidence here is not conclusive because most of the simulations are offset from the melting temperatures by several Kelvins and because our definition of a local structure factor includes an average over several molecular rows.

The melting curve of the submonolayer N_2/graphite system has been discussed as an example of an "incipient triple point system."[23] The strong correlation that we find between the activation of defects in the submonolayer solid and its melting produces a rather different picture than the modeling, which has emphasized the modulation of the fluid phase.[24] Here, the plateau in the melting curve is associated with a temperature of mixing of vacancies and molecules. The fluid phase has not been analyzed, so we cannot comment on the existence of a liquid-vapor coexistence region.

At low coverages, the roughness of the edges completely penetrates small patches at a lower temperature resulting in a lower melting point, which further decreases with decreasing coverage. Since this melting temperature reflects the size of the patches, it may be used to gauge the coherence length of the substrate.

We have found a small change in the azimuthal angle disorder transition temperature from 22 K in the complete monolayer to 18 K in submonolayer films. The reason for that drop in the transition temperature is not as well understood as the melting transition because it has been more difficult to analyze the data. However, the

scenario from the melting transition also seems to apply here. The azimuthal angle disorder is initiated in the region of the edges of the patch and propagates into the patch interior at the disorder transition temperature. In the narrowest patches, the azimuthal transition disorder temperature is very low, less than 5 K.

There is a serious flaw in the potential model. The calculated melting points are generally too low and an analysis has shown that the problem may be caused by an improper representation of the McLachlan surface-mediation term. No solution to the problems has yet been offered. It is important to realize that although the quantitative agreement between experiments and simulations is poor, there is no reason to believe that our qualitative understanding of the melting process will change with a more adequate potential.

ACKNOWLEDGMENTS

We thank Professors R. D. Etters and B. Kuchta for very helpful and open discussions of their work. Our work was partially supported by the National Science Foundation under Grants Nos. DMR-9314235 (H.T.) and DMR-9120199 (L.W.B.) and by the Danish Natural Science Foundation (F.Y.H.).

[1] T. T. Chung and J. G. Dash, Surf. Sci. **66**, 559 (1977).
[2] M. H. W. Chan, A. D. Migone, K. D. Miner, and Z. R. Li, Phys. Rev. B **30**, 2681 (1984).
[3] M. H. W. Chan, in *Phase Transitions in Surface Films 2*, edited by H. Taub, G. Torzo, H. J. Lauter, and S. C. Fain, Jr. (Plenum, New York, 1991), pp. 1–10.
[4] M. T. Alkhafaji and A. D. Migone, Phys. Rev. B **48**, 1761 (1993); A. D. Migone (private communication).
[5] F. Y. Hansen and H. Taub, Phys. Rev. Lett. **69**, 652 (1992); G. J. Trott, Ph.D. thesis, University of Missouri-Columbia, 1981.
[6] R. D. Etters, B. Kuchta, and J. Belak, Phys. Rev. Lett. **70**, 826 (1993); M. Roth and R. D. Etters, Phys. Rev. B **44**, 6581 (1991); R. D. Etters, M. W. Roth, and B. Kuchta, Phys. Rev. Lett. **65**, 3140 (1990); B. Kuchta and R. D. Etters (unpublished).
[7] Y. P. Joshi and D. J. Tildesley, Mol. Phys. **55**, 999 (1985).
[8] F. Y. Hansen and L. W. Bruch, Phys. Rev. B **51**, 2515 (1995).
[9] F. Y. Hansen, J. C. Newton, and H. Taub, J. Chem. Phys. **98**, 4128 (1993).
[10] M. A. Moller and M. L. Klein, Chem. Phys. **129**, 235 (1989); see also A. Cheng and M. L. Klein, Langmuir **8**, 2798 (1992).
[11] V. R. Bhethanabotla and W. A. Steele, Langmuir **3**, 581 (1987); Can. J. Chem. **66**, 866 (1988); Phys. Rev. B **41**, 9480 (1990).
[12] We follow the suggestion of M. Wortis, in *Phase Transitions in Surface Films* (Ref. 3), pp. 471–487 for the use of the term "atomic roughening." We use it to denote a situation with a significant number of vacancies and other short-range structural disorder on an otherwise perfect patch. This is distinct from the condition termed "thermodynamic roughening," which has a divergent height-height correlation function.
[13] C. S. Murthy, K. Singer, M. L. Klein, and I. R. McDonald, Mol. Phys. **41**, 1387 (1980).
[14] A. D. McLachlan, Mol. Phys. **7**, 381 (1964); L. W. Bruch, J. Chem. Phys. **79**, 3148 (1983).
[15] W. A. Steele, J. Phys. (Paris) Colloq. **38**, C4-61 (1978).
[16] W. E. Carlos and M. W. Cole, Surf. Sci. **91**, 339 (1980).
[17] F. Y. Hansen, L. W. Bruch, and S. E. Roosevelt, Phys. Rev. B **45**, 11 238 (1992).
[18] M. P. Allen and D. J. Tildesley, *Computer Simulation of Liquids* (Clarendon Press, Oxford, 1987).
[19] B. Kuchta and R. D. Etters, Phys. Rev. B **36**, 3400 (1987).
[20] B. Kuchta and R. D. Etters (private communication).
[21] M. J. Bojan and W. A. Steele, Langmuir **3**, 116 (1987).
[22] D. M. Zhu, D. Pengra, and J. G. Dash, Phys. Rev. B **37**, 5586 (1988).
[23] A. D. Migone, M. H. W. Chan, K. J. Niskanen, and R. B. Griffiths, J. Phys. C **16**, L1115 (1983).
[24] K. J. Niskanen and R. B. Griffiths, Phys. Rev. B **32**, 5858 (1985); K. J. Niskanen, *ibid.* **33**, 1830 (1986); L. M. Sander and J. Hautman, *ibid.* **29**, 2171 (1984).